Polarimetric Decompositions of Temperate Wetlands at C-Band

Brian Brisco, Frank Ahern, Sang-Hoon Hong, *Member, IEEE*, Shimon Wdowinski, Kevin Murnaghan, Lori White, and Donald K. Atwood, *Member, IEEE*

***Abstract*—C-band SAR is well established as a useful sensor for water resources applications. It is commonly accepted that the backscatter from wetlands that consist of many emergent stems over open water (swamps and marshes) is dominated by a double-bounce scattering mechanism. However, recent observations with fully polarimetric data from Radarsat-2 over the extensive wetlands of the Everglades and numerous small wetlands in Ontario appear to be inconsistent with this interpretation of the backscatter physics. In this paper, we use several forms of polarimetric analysis and decomposition. All of these indicate that the backscatter from small marshes and swamps in Ontario is dominated by polarimetric characteristics normally attributed to the odd-bounce mechanism. This anomalous result might be explained as a consequence of changes in the double-bounce reflectance properties of vegetation as a function of the incidence angle. However, detailed electromagnetic backscatter modeling will be needed to provide a more complete and reliable understanding of the details of backscattering from wetlands with emergent vegetation. Additional observational and theoretical work will be required to document and understand the unusual results we report here. If these results are substantiated, the SAR community must re-interpret the generally accepted meanings of the popular decomposition variables, and introduce new terminology to describe them. This would lead to an improved understanding of the backscatter physics and better use of polarimetric SAR for wetland management applications.**

***Index Terms*—Polarimetric radar, synthetic aperture radar (SAR), water resources.**

Manuscript received September 19, 2014; revised November 29, 2014; accepted December 24, 2014. Date of publication April 08, 2015; date of current version August 11, 2015. The work of S. Wdowinski and S.-H. Hong was supported by NASA Cooperative Agreement NNX10AQ13A (WaterSCAPES: Science of Coupled Aquatic Processes in Ecosystems from Space) and the Florida Coastal Everglades Long-Term Ecological Research Program under National Science Foundation Grant DEB-1237517. This paper was presented at the 2014 meeting of the International Geoscience and Remote Sensing Society/35th Canadian Symposium on Remote Sensing at Québec, Canada, July 2014.

B. Brisco is with the Canada Centre for Mapping and Earth Observation, Natural Resources Canada, Ottawa, ON K1S 5K2, Canada (e-mail: brian.brisco@nrcan.gc.ca).

F. Ahern is with TerreVista Earth Imaging, Cormac, ON K0J 1M0, Canada (e-mail: frank.ahern.g@gmail.com).

S.-H. Hong is with the Division of Polar Ocean Environment, Korea Polar Research Institute, Incheon, Korea (email: shong@kopri.re.kr), and also with the Department of Marine Geosciences, University of Miami, Miami, FL 33149-1098 USA (e-mail: shong@rsmas.miami.edu).

S. Wdowinski is with the Department of Marine Geosciences, University of Miami, Miami, FL 33149-1098 USA (e-mail: shimonw@rsmas.miami.edu).

K. Murnaghan and L. White are with the Earth Observation and GeoSolutions Division, Canada Centre for Mapping and Earth Observation, Ottawa, ON K1S 5K2, Canada.

D. Atwood is with the Michigan Tech Research Institute, Ann Arbor, MI 48105-1579 USA (e-mail: dkatwood@mtu.edu).

Color versions of one or more of the figures in this paper are available online at http://ieeexplore.ieee.org.

Digital Object Identifier 10.1109/JSTARS.2015.2414714

I. Introduction

IT IS WELL known that wetlands play a vital role in the water cycle. They help control water flow, improve water quality by filtering out impurities, and provide vital habitat for a variety of plants and animals. Wetlands can also be important for local recreational activities including hiking, hunting, fishing, bird-watching, swimming, and boating. Many other human activities and ecosystem functions can be attributed to wetlands. They are thus important for a variety of reasons including the quality of life for humans. However, wetlands are under pressure due to land-use and climate change, resulting in fragmentation and drainage to accommodate farming or other development activities. It is therefore important to monitor the health of existing wetlands and attempt to manage them in a sustainable fashion.

SAR has proven to be an effective tool for water resource applications and is used operationally for flood and surface water [1]–[3]. The timely data acquisition capabilities and sensitivity to water make it an attractive sensor for these applications to time the data collection to the flood event or to the water cycle. SAR has also proven useful for wetland classification alone or in combination with optical data [4]–[8] and is particularly useful for mapping flooded vegetation because of the canopy penetration and subsequent interaction with the underlying water surface [9]–[12]. A detailed review of the use of SAR for detecting and characterizing wetlands is provided in [13].

As a result of increasing concern with water resources, the Canada Centre for Mapping and Earth Observation (CCMEO, formerly CCRS) has undertaken a water resource program. Part of this program has included interferometric and polarimetric observations of wetlands with the Radarsat-2 C-band SAR. Under this program, researchers at the University of Miami have been collaborating with CCMEO with Radarsat-2 studies of the Florida Everglades. While working with polarimetric data, both teams found that the generally accepted interpretation of microwave backscatter from wetlands does not seem to be supported by the observational data [14], [15]. In particular, the large increase in backscattered power observed in wetlands (reviewed in [9] and [13]) has been long considered a result of the double-bounce backscattering mechanism [16], yet polarimetric decompositions have indicated that the return is dominated by the single- (or odd)-bounce mechanism.

The inconsistency between the inferred double-bounce scattering mechanism and the results of some polarimetric decompositions suggests either that the inferred mechanism is incorrect, or that double bounce in wetlands is more complicated

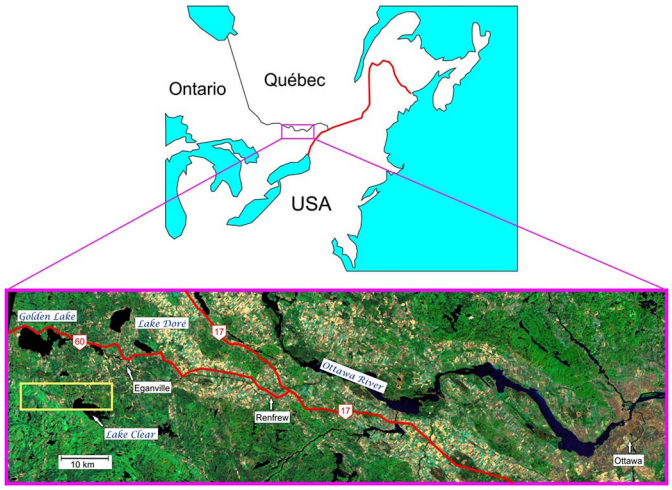

Fig. 1. Study area in the upper Ottawa Valley. The magenta frame spanning the Ottawa River (the border between Québec and Ontario) shows the location of the annotated Landsat image insert, whereas the yellow box in the left side of the Landsat image outlines our study area.

and subtle than previously thought. Double-bounce backscatter may exhibit anomalous polarimetric properties that are not consistent with existing decomposition theory [14], [17]. This paper describes our new observations, the problems they present for the generally accepted interpretation of double-bounce backscatter, and proposes opportunities for further work to address the identified anomalies.

II. Methodology

The results reported here were derived from Radarsat-2 polarimetric data acquired over a test site in the Upper Ottawa Valley during three dates in 2011: June 14, September 18, and November 5. Several polarimetric analysis techniques were employed.

A. Study Area

The test area lies mainly in the southern portion of the Upper Ottawa Valley. This part of the valley is defined, geomorphologically, by the Ottawa-Bonnechere graben. Except for isolated areas where the pre-Cambrian shield protrudes in hills of several tens of meters in height, the topography is subdued. The surficial material is primarily glacial till, occasionally sculpted into eskers and kames, but often relatively poorly drained. Wetlands are common, generally formed by beaver floods, and many of the swamps are populated by trees that have died as a result of the flooding. These are commonly monocultures, or near-monocultures of black ash (*Fraxinus nigra*), eastern white cedar (*Thuja occidentalis*), tamrarack (*Larix laricina*), or speckled alder (*Alnus incana*), depending on the soil and moisture conditions when the stand was established before flooding. Most of the marshes are covered with live herbaceous plants, typically cattails (*Typha* spp.), sedges (*Carex* spp.), and grasses (*Poaceae* spp.) (Fig. 1).

TABLE I
Geometric Characteristics of the Radarsat-2 Spotlight and FQ3 Data Used in This Study

Parameter	Spotlight	FQ3
Polarization	HH	Full polarimetry
Incidence angle	46.6°	21.9°
Image size (km)	18 (R) x 8 (Az)	25 x 25
Slant range resolution (m)	1.6	5.2
Slant range pixel spacing (m)	1.3	4.7
Ground range resolution (m)	2.2	13.9
Ground range pixel spacing (m)	1.8	12.5
Azimuth resolution (m)	0.8	7.6
Azimuth pixel spacing (m)	0.4	5.1

B. Radarsat-2 Data

The first Radarsat-2 data used for this project consisted of five Spotlight Mode scenes acquired from June to October 2010. These were processed as interferometric pairs, which enabled us to identify a sample of wetlands that exhibited high coherence, and interferometric phase changes that appeared to be related to changes in water level. The interferometric work has continued, but is not reported here. The Radarsat-2 data for this polarimetric study were acquired during the growing season of 2011, on June 14, September 18, and November 5, in the FQ3 beam mode. The geometric characteristics are provided in Table I. The steep incidence angle of the FQ3 mode results in a ground range resolution considerably larger than the slant range resolution. The data were processed into single-look-complex (SLC) images to provide the input data necessary for polarimetric studies.

C. Land Cover Types

Although we are interested primarily in the polarimetric backscatter characteristics of wetlands, it is important to compare these with the polarimetric backscatter characteristics of other land cover types whose backscatter characteristics have been extensively studied and reported. In addition to swamps and marshes, we extracted backscatter characteristics for open-water bodies, open fields, and conifer (red pine, *Pinus rubra*) plantations.

We first used the interferometric pairs to identify a large sample of candidate wetlands, which was reduced to an initial sample of 20 wetlands where swamp (tree) vegetation covered the majority of the wetland and 12 wetlands where marsh (herbaceous) vegetation covered the majority of the wetland. To ensure reliable results, we reviewed the sample and eliminated wetlands that were small enough that registration errors might compromise the results. We also redefined the wetland boundaries using very high-resolution (20 cm) optical data to eliminate open water and marsh areas in wetlands that were predominantly swamps, and to eliminate open water and swamp areas in wetlands that were predominantly marshes. Our final sample contained 10 swamps and 8 marshes, totaling 3096

pixels or 1974 ha of land cover as swamp, and 1620 pixels or 1033 ha of land cover as marsh.

We selected nine small-to-medium-sized lakes for our sample of water bodies. We avoided the larger lakes in our area because they are more subject to the effects of wind, and we wanted to obtain statistics from flat water.

We selected 11 open fields in the area around Cormac, Ontario. The soil in this area is relatively poor, so these fields are used for hay and pasture.

We selected eight uniform polygons with red pine plantations in the area immediately to the northwest of Lake Clear. These are all stands of uniformly spaced trees of the same age (approximately 40–50 years) and similar heights. Their appearance on the radar imagery is very uniform, and we avoided any irregularities in the stands when drawing polygon boundaries.

D. Data Analysis

In order to avoid resampling that might alter the speckle statistics, we created a set of polygons for our land cover samples in the UTM system, and reprojected the polygons back to the coordinate system of each image.

We determined the mean image intensity, and the standard error of the mean, in linear (not db) units of backscatter cross section (σ^0) for all of the pixels of each land cover type. We then performed various polarimetric decompositions and analyzed the outputs as a function of these land cover types. The decompositions required spatial filtering to reduce speckle noise, as described in Section II-D7. We also added the intensities of all of the components of each decomposition and compared this with the sum of the intensities of four polarimetric channels, to make sure we avoided procedural or computational errors.

Because our results are unexpected and will require new thinking about the backscatter process, we are documenting our processing methods thoroughly in this paper.

1) Original Intensity Channels: The original intensity channels are called HH, HV, VH, and VV, where H and V are used to represent horizontal and vertical transmitted and received radar energy. In the Single Look Complex product, each pixel of a given polarization channel is a complex number $\mathrm{XY} = \mathrm{XY_r} + \mathrm{iXY_i}$ with a real part $\mathrm{XY_r}$ and an imaginary part $\mathrm{XY_i}$. X and Y, the transmit and receive polarizations, can be replaced by the four permutations of H and V.

The four channels are also equal to the four elements of the complex scattering matrix $\mathbf{S}$

$$\mathbf{S} = \begin{bmatrix} S_{HH} & S_{HV} \\ S_{VH} & S_{VV} \end{bmatrix}$$

where each of the elements of $\mathbf{S}$ is a complex number. The pixel intensity of each channel equals the amplitude of the complex backscatter: $\mathrm{Ixy} = (\mathrm{Srxy}^2 + \mathrm{Sixy}^2)$ where Srxy is the real part of the scattering matrix element Sxy, Sixy is the imaginary part, and xy represents the transmitted and received polarizations.

2) HH–VV Phase: The HH–VV phase provides important diagnostic information about the different scattering mechanisms that contribute to the total backscatter of a target [16]–[18]. From decomposition theory, odd-bounce backscatter results in HH–VV phase values near 0°, even-bounce backscatter results in HH–VV phase values near 180°, while volume scattering results in random HH–VV phase values, uniformly distributed from $-180°$ to 180°. Thus this "co-pol phase difference" offers a useful tool for investigating whether Polarimetric Pauli Coherency Matrix polarimetric results are consistent with the assumed scattering mechanisms.

3) Polarimetric Pauli Coherency Matrix: The diagonal elements of the Polarimetric Pauli Coherency Matrix [18] are: $\mathrm{P}_{11} = \langle|\mathrm{S_{HH}} + \mathrm{S_{VV}}|^2\rangle$; $\mathrm{P}_{22} = \langle|\mathrm{S_{HH}} - \mathrm{S_{VV}}|^2\rangle$; $\mathrm{P}_{33} = 4\langle|\mathrm{S_{HV}}|^2\rangle$, where the angle brackets indicate an ensemble average and the straight brackets indicate the amplitudes of complex numbers. This transformation of the data can be considered a decomposition [19], with the first component representing the contribution of odd-bounce backscatter, the second component representing the contribution of even-bounce backscatter, and the third component corresponding to a dihedral oriented at 45°, and could be associated with volume scattering. The Pauli decomposition is energy conserving in the sense that the sum of the three diagonal elements equals the total backscatter cross section of the return signal.

4) Freeman–Durden Decomposition: The Freeman–Durden (F–D) decomposition [20] is one of the earliest polarimetric decompositions that produced three features that are attributed to single bounce, double bounce, and volume scattering. First, the volume scattering component is determined directly from the intensity of the cross-polarized channels. Next, a test is applied that chooses between double bounce and surface scatter as the dominant effect, on a per-pixel basis. This test is a test of the sign of $\theta_{HH} - \theta_{VV}$, the co-pol phase difference. It will assign pixels to single-bounce scattering for phase angles from 0° to 90° and from 270° to 360°, and double-bounce for phase angles between 90° and 270°. This means that the output does not represent a smooth mathematical transformation of the data, but can exhibit sudden jumps that appear as artifacts in images of the F–D components. In our imagery, these are particularly notable in the image that corresponds to the double-bounce component. These consist of isolated pixels, or small groups of pixels, which have intensities that are greatly different from their surroundings not related to changes in ground cover. In gray-scale imagery, this type of artifact is often called salt-and-pepper noise. The F–D decomposition is intended to be energy conserving, but minor variations are introduced through its production of the artifacts described above.

5) H–W Decomposition: The Hong–Wdowinski (H–W) four-component decomposition is an extension of the F–D decomposition, in which a backscatter component modeled as a rotated dihedral is added as a fourth component [14]. This was done because the Miami Radarsat-2 data of the Everglades showed sufficient coherence to produce interpretable phase changes ("fringes") in HV imagery. In fact, the HV fringes were very similar to the HH and VV fringes, indicating that all three channels included an interaction with the water surface, and that changes in the elevation of the water surface between two dates were the dominant source of phase change in all three images.

Like the F–D decomposition, the H–W decomposition implemented a choice between double bounce and surface scatter as the dominant effect, on a per-pixel basis. Similarly, the output does not represent a smooth mathematical transformation of the data, and can exhibit sudden jumps that appear as artifacts in images of the components. In our imagery, the fourth (rotated dihedral) component consists entirely of artifacts, and was not used. This is likely a consequence of the software decision that surface scattering dominates, resulting in a negligible contribution by the rotated dihedral component. The component representing even-bounce backscatter exhibited numerous isolated bright pixels that contribute to a high variance in the statistics. The component representing volume scattering also exhibits numerous artifacts, but these are not as pronounced. The H–W decomposition is intended to be energy conserving, but as in the case of the F–D decomposition, minor variations are introduced through its production of artefacts similar to those produced by F–D.

6) m-chi Decomposition: The m-chi decomposition has been proposed [21] as a polarimetric transformation of the data that can be used in conjunction with so-called Compact Polarimetry [22].

The features are defined as

$$\mathrm{B} = < \mathrm{m}\mathrm{S}_1 \left(1 - \sin 2\chi\right)/2 >^{1/2};$$
$$\mathrm{R} = < \mathrm{m}\mathrm{S}_1 \left(1 + \sin 2\chi\right)/2 >^{1/2};$$
$$\mathrm{G} = < \mathrm{S}_1 \left(1 - \mathrm{m}\right) >^{1/2}.$$

These features are designed to reproduce images similar in appearance to earlier representations of decompositions (van Zyl [16], Freeman–Durden [20], and Yamaguchi *et al.* [23]), in which single bounce is displayed as blue (B), double bounce is displayed as red (R), and volume scattering is displayed as green (G). In these equations $\mathrm{S}_1 = |\mathrm{S}_{\mathrm{HH}}|^2 + |\mathrm{S}_{\mathrm{VV}}|^2$, the first Stokes parameter (also referred to as S0 by some sources) $\mathrm{m} =$ the degree of polarization, and χ is the Poincaré ellipticity parameter. Although the use of square root compensates to a certain extent for the large dynamic range of typical SAR data and produces attractive-looking images, for this work, we chose to leave out this square-root compression and keep our data in linear units proportional to backscattered intensity. Also note that the difference in sign between the equations for B and R is dependent on assumptions about the transmitted polarization and the sign convention for the scattering mechanism.

Because the m-chi decomposition is implemented as a mathematical transformation of the original data, no assumptions or logical decisions are required, so this decomposition is not subject to producing artifacts. The m-chi decomposition is expected to be energy conserving.

7) Number of Independent Samples and Standard Error of the Mean: With the exception of the original polarimetric data, all of the other data representations that we employed require spatial filtering to decrease speckle noise. Our filtering consisted of an average of every two lines of data in the azimuth direction to compensate for the large difference between azimuth and ground-range pixel spacing for data visualization, followed by a 5×5 boxcar filter, to produce an equivalent 5×10 or 50-look estimate for each pixel.

The standard error of the mean is calculated from

$$SEM = \sqrt{\frac{var}{N_{\mathrm{ind}}}};$$

where var is the variance of the mean value and N_{ind} is the number of independent samples.

In the cases where we have implemented spatial averaging to decrease the variance of the image data, $N_{\mathrm{ind}} = \mathrm{Nc}/50$ where $\mathbf{N}\mathrm{c}$ is the number of pixels of class c that was used to calculate the mean, because each output pixel represents a 5×10 average of original pixels.

III. Results and Discussion

A. Original Intensity Channels and Total Energy

The backscatter from the original bands does not present any surprises. The intensities in HH and VV are similar for the water, open fields, and pine plantations, but not for marshes and swamps, where HH is considerably greater than VV [see Fig. 2(a)–(c)]. This is consistent with a large body of literature, as summarized in [9] and [13]. The cross-polarized backscatter is typically about 8%–30% as strong as the combined HH + VV backscatter, with the pine type having larger values. This is consistent with the expectation of larger amounts of volume scattering in the live canopy.

Many of the land cover types exhibit decreases in backscatter from June to September to November, likely a result in decreasing moisture in plants and soil. The backscatter of water is affected by wind in ways, i.e., very sensitive to wind speed, wind direction, and fetch, so we cannot comment meaningfully on temporal changes in the backscatter of water, except to note that it is always the lowest, or one of the lowest, of the land cover classes.

B. HH–VV Phase

The phase difference between HH and VV backscatter is an important diagnostic tool, as described in Section II-D2. In order to provide an additional check on our decomposition analyses, we have calculated the histograms of the polarimetric phase for the June data. These are shown in Fig. 3(a)–(e).

We see that the backscatter from water is tightly distributed near 0°, which is consistent with water as a single-bounce scatterer. Much of the dispersion in the histogram will be the result of the random phase effects of coherent speckle. Open fields are also centered near 0°, but with a wider distribution, which could indicate a slightly greater amount of higher order scattering. The pine plantation histogram remains centered near 0°, but exhibits a larger proportion of pixels with large phase values, indicating an increase in the amount of higher order scattering. The marsh and swamp histograms are also centered near 0°, with a distribution away from zero that is similar to that of the open fields, and smaller than that of the pine plantations.[1]

[1]The peaks of the distributions for the Field, Marsh, and Swamp classes are offset from zero degrees. However, the number of independent samples for these distributions is small enough that these offsets are not statistically significant at high confidence levels.

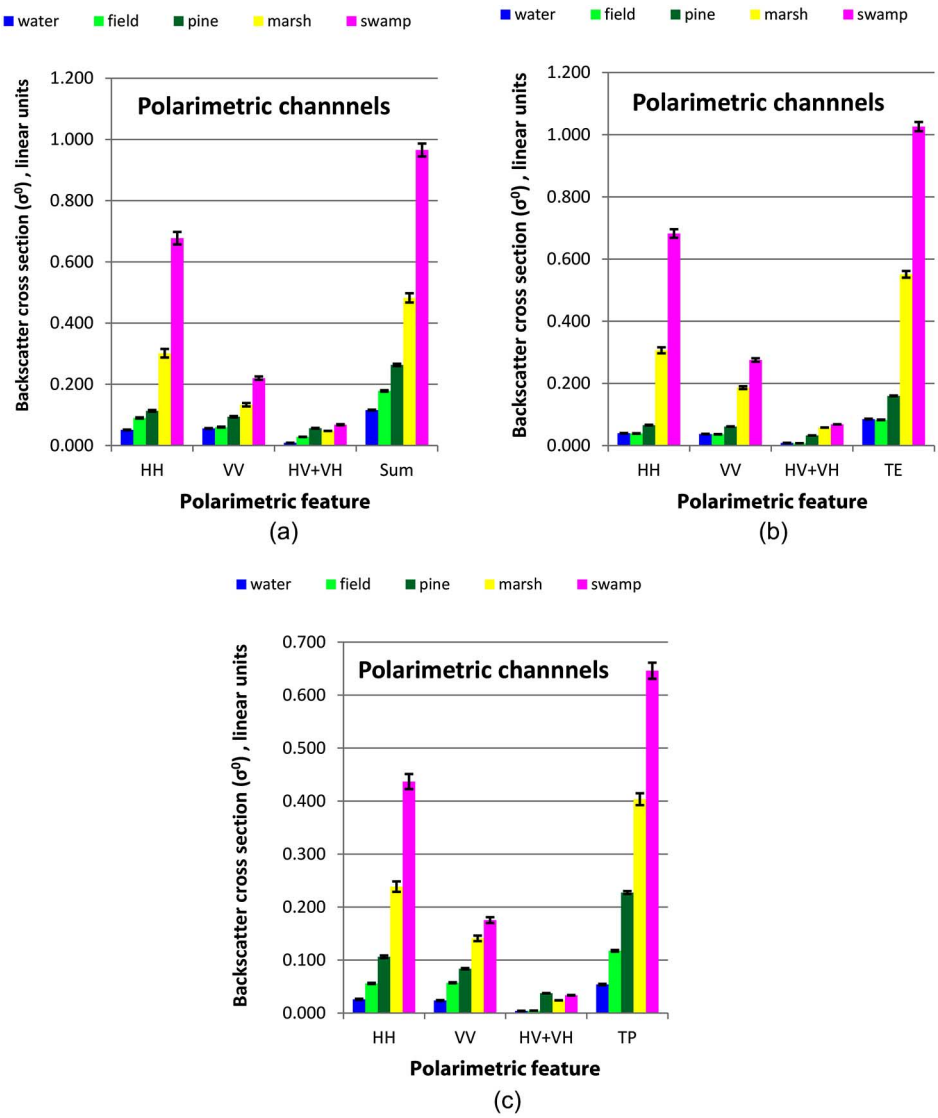

Fig. 2. Backscatter from original polarimetric channels acquired: (a) June 14, 2011; (b) September 18, 2011; (c) November 05, 2011.

This is unexpected. We expected to see a larger proportion of the pixels to have HH–VV phase values between 90° and 270°, diagnostic of double-bounce backscatter. Since the water level in wetlands can be monitored with interferometry [14], this indicates that microwaves must coherently reflect off the water. It is hard to conceive of any mechanism except double bounce that could do this. This unexpected result is explored in more detail using the Pauli coherency matrix and three polarimetric decompositions described in Section II.

C. Pauli Coherency Matrix and Polarimetric Decompositions

Our numerical results are presented in Tables II–IV, for the three dates in 2011: June 14, September 18, and November 5. The three polarimetric features extracted from each decomposition are labeled as odd bounce, even bounce, and volume scattering.

We will discuss the June results first, and the September and November results as a comparison. First, note that the backscatter cross-sectional sums, in linear units, agree with each other quite well. The backscatter cross-sectional sums, in db units, agree with published values, providing confidence in our radiometric calibration.

For water, all of the decompositions indicate that a large fraction of the backscattered power comes from odd bounce, which we can confidently associate with single-bounce backscatter. For the open field and pine plantation cover types, there is a surprising variability of the fraction of backscatter attributed to volume scattering by the different decompositions, with the Freeman–Durden and m-chi decompositions producing higher values than Pauli and Hong–Wdowinski. This is related to the details of the models and beyond the scope of this investigation.

The anomaly that concerns us the most is the very small fraction of backscatter from marshes and swamps assigned to even bounce, which is normally attributed to the double-bounce mechanism. This is a concern because we are confident that the microwaves are interacting with both the water surface and the vegetation, as indicated by the HH-to-VV intensity ratio, and especially by the high interferometric coherence and phase changes observed with the Spotlight Mode data.

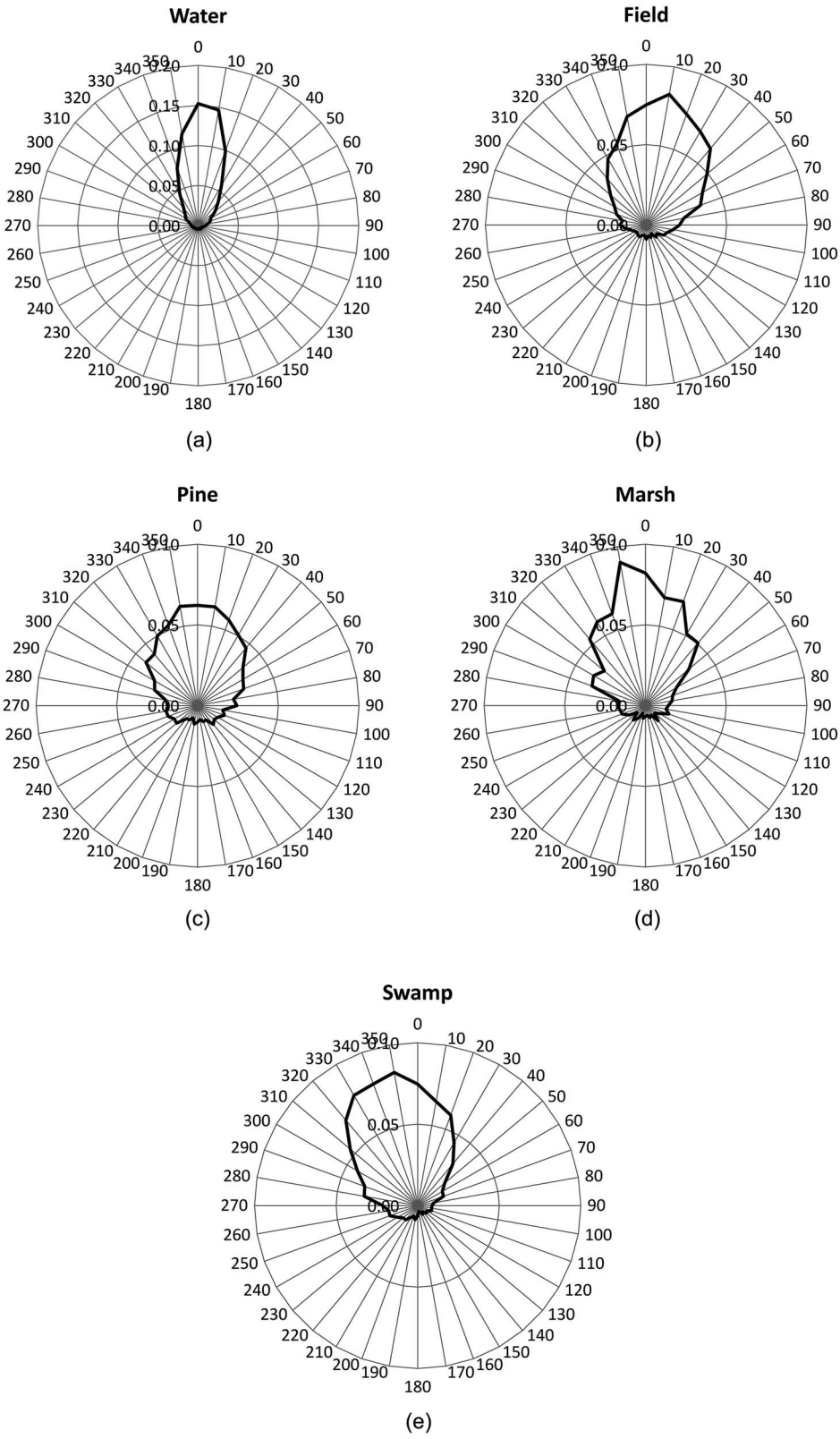

Fig. 3. (a) HH–VV phase for water. The envelope of the histogram, in 10° intervals is shown in black. The radial scale indicates the frequency for each bin, normalized to the total number of samples. The azimuth scale indicates these 10° intervals, beginning with 0° and continuing clockwise. All of the phase plots are for the June 2011 data. (b) HH–VV phase for open fields. (c) HH–VV phase for red pine plantations. (d) HH–VV phase for marshes (herbaceous vegetation emergent from water). (e) HH–VV phase for swamps (woody vegetation emergent from water).

TABLE II
BACKSCATTER CROSS-SECTIONS (σ^0) FOR JUNE; LINEAR UNITS

		Odd bounce		Even bounce		Volume scattering		Sum		Fractional backscatter		
Cover	Decomp	mean	s.e.m	mean	s.e.m	mean	s.e.m	linear	db	Odd	Even	Vol
Water	Pauli	0.095	0.004	0.017	0.001	0.010	0.001	0.122	−9.15	0.78	0.14	0.08
Water	FD	0.099	0.004	0.008	0.001	0.057	0.005	0.164	−7.84	0.60	0.05	0.35
Water	HW	0.104	0.003	0.024	0.013	0.024	0.001	0.151	−8.20	0.69	0.16	0.16
Water	m-chi	0.087	0.002	0.004	0.000	0.046	0.002	0.136	−8.65	0.64	0.03	0.33
Field	Pauli	0.116	0.004	0.037	0.001	0.029	0.001	0.181	−7.41	0.64	0.20	0.16
Field	FD	0.068	0.004	0.006	0.001	0.119	0.005	0.192	−7.17	0.35	0.03	0.62
Field	HW	0.076	0.003	0.073	0.013	0.051	0.001	0.200	−6.99	0.38	0.37	0.26
Field	m-chi	0.065	0.002	0.013	0.000	0.104	0.002	0.182	−7.40	0.36	0.07	0.57
Pine	Pauli	0.151	0.015	0.062	0.003	0.056	0.002	0.269	−5.70	0.56	0.23	0.21
Pine	FD	0.039	0.004	0.010	0.001	0.210	0.000	0.259	−5.86	0.15	0.04	0.81
Pine	HW	0.074	0.005	0.053	0.027	0.113	0.007	0.240	−6.19	0.31	0.22	0.47
Pine	m-chi	0.046	0.000	0.019	0.001	0.183	0.003	0.248	−6.05	0.18	0.08	0.74
Marsh	Pauli	0.327	0.015	0.110	0.003	0.050	0.002	0.486	−3.13	0.67	0.23	0.10
Marsh	FD	0.304	0.004	0.036	0.001	0.262	0.000	0.602	−2.21	0.51	0.06	0.44
Marsh	HW	0.375	0.005	0.099	0.027	0.126	0.007	0.599	−2.23	0.63	0.16	0.21
Marsh	m-chi	0.284	0.000	0.060	0.001	0.247	0.003	0.591	−2.29	0.48	0.10	0.42
Swamp	Pauli	0.637	0.042	0.260	0.023	0.069	0.003	0.966	−0.15	0.66	0.27	0.07
Swamp	FD	0.673	0.033	0.097	0.010	0.303	0.010	1.073	0.31	0.63	0.09	0.28
Swamp	HW	0.764	0.024	0.212	0.166	0.145	0.008	1.120	0.49	0.68	0.19	0.13
Swamp	m-chi	0.538	0.017	0.187	0.010	0.373	0.008	1.098	0.41	0.49	0.17	0.34

TABLE III
BACKSCATTER CROSS-SECTIONS (σ^0) FOR SEPTEMBER; LINEAR UNITS

		Odd bounce		Even bounce		Volume scattering		Sum		Fractional backscatter		
Cover	Decomp	mean	s.e.m	mean	s.e.m	mean	s.e.m	linear	db	Odd	Even	Vol
Water	Pauli	0.066	0.006	0.015	0.003	0.009	0.002	0.091	−10.41	0.73	0.17	0.10
Water	FD	0.038	0.002	0.005	0.000	0.024	0.001	0.067	−11.72	0.57	0.07	0.36
Water	HW	0.056	0.000	0.021	0.002	0.018	0.001	0.096	−10.19	0.59	0.22	0.19
Water	m-chi	0.047	0.001	0.006	0.000	0.042	0.001	0.095	−10.24	0.50	0.06	0.44
Field	Pauli	0.065	0.006	0.011	0.003	0.008	0.002	0.084	−10.73	0.78	0.13	0.09
Field	FD	0.046	0.002	0.003	0.000	0.027	0.001	0.077	−11.16	0.61	0.04	0.35
Field	HW	0.057	0.000	0.011	0.002	0.014	0.001	0.083	−10.82	0.69	0.13	0.18
Field	m-chi	0.048	0.001	0.001	0.000	0.036	0.001	0.085	−10.69	0.56	0.02	0.42
Pine	Pauli	0.092	0.004	0.036	0.001	0.032	0.001	0.160	−7.95	0.57	0.23	0.20
Pine	FD	0.027	0.002	0.006	0.000	0.130	0.000	0.163	−7.88	0.17	0.04	0.80
Pine	HW	0.054	0.005	0.042	0.053	0.067	0.005	0.163	−7.87	0.33	0.26	0.41
Pine	m-chi	0.035	0.000	0.012	0.001	0.114	0.000	0.161	−7.92	0.22	0.08	0.71
Marsh	Pauli	0.376	0.004	0.097	0.001	0.057	0.001	0.530	−2.76	0.71	0.18	0.11
Marsh	FD	0.273	0.002	0.023	0.000	0.209	0.000	0.505	−2.97	0.54	0.05	0.41
Marsh	HW	0.317	0.005	0.099	0.053	0.107	0.005	0.524	−2.81	0.61	0.19	0.20
Marsh	m-chi	0.256	0.000	0.028	0.001	0.233	0.000	0.517	−2.87	0.50	0.05	0.45
Swamp	Pauli	0.704	0.044	0.217	0.025	0.067	0.005	0.988	−0.05	0.71	0.22	0.07
Swamp	FD	0.624	0.035	0.073	0.006	0.251	0.005	0.948	−0.23	0.66	0.08	0.26
Swamp	HW	0.699	0.013	0.159	0.133	0.125	0.007	0.984	−0.07	0.71	0.16	0.13
Swamp	m-chi	0.523	0.009	0.105	0.006	0.354	0.005	0.982	−0.08	0.53	0.11	0.36

TABLE IV
BACKSCATTER CROSS-SECTIONS (σ^0) FOR NOVEMBER; LINEAR UNITS

		Odd bounce		Even bounce		Volume scattering		Sum		Fractional backscatter		
Cover	Decomp	mean	s.e.m	mean	s.e.m	mean	s.e.m	linear	db	Odd	Even	Vol
Water	Pauli	0.044	0.004	0.010	0.002	0.005	0.001	0.059	–12.29	0.75	0.17	0.08
Water	FD	0.030	0.002	0.004	0.000	0.015	0.001	0.049	–13.10	0.61	0.08	0.31
Water	HW	0.040	0.000	0.016	0.002	0.010	0.000	0.066	–11.80	0.61	0.24	0.15
Water	m-chi	0.033	0.000	0.003	0.000	0.024	0.000	0.059	–12.26	0.55	0.05	0.40
Field	Pauli	0.107	0.004	0.008	0.002	0.005	0.001	0.120	–9.21	0.89	0.07	0.04
Field	FD	0.096	0.002	0.003	0.000	0.018	0.001	0.117	–9.32	0.82	0.03	0.15
Field	HW	0.102	0.000	0.012	0.002	0.009	0.000	0.123	–9.10	0.83	0.10	0.07
Field	m-chi	0.094	0.000	0.001	0.000	0.025	0.000	0.120	–9.21	0.79	0.01	0.21
Pine	Pauli	0.146	0.005	0.045	0.002	0.037	0.001	0.228	–6.42	0.64	0.20	0.16
Pine	FD	0.072	0.004	0.008	0.001	0.152	0.000	0.232	–6.35	0.31	0.03	0.66
Pine	HW	0.100	0.009	0.070	0.061	0.069	0.007	0.239	–6.22	0.42	0.29	0.29
Pine	m-chi	0.074	0.000	0.012	0.001	0.145	0.000	0.231	–6.37	0.32	0.05	0.63
Marsh	Pauli	0.319	0.005	0.047	0.002	0.025	0.001	0.391	–4.08	0.82	0.12	0.06
Marsh	FD	0.281	0.004	0.011	0.001	0.090	0.000	0.382	–4.18	0.74	0.03	0.24
Marsh	HW	0.293	0.009	0.094	0.061	0.044	0.007	0.431	–3.66	0.68	0.22	0.10
Marsh	m-chi	0.265	0.000	0.017	0.001	0.113	0.000	0.395	–4.04	0.67	0.04	0.29
Swamp	Pauli	0.482	0.038	0.113	0.020	0.034	0.002	0.629	–2.01	0.77	0.18	0.05
Swamp	FD	0.459	0.032	0.032	0.008	0.132	0.003	0.623	–2.06	0.74	0.05	0.21
Swamp	HW	0.481	0.007	0.074	0.019	0.063	0.002	0.618	–2.09	0.78	0.12	0.10
Swamp	m-chi	0.395	0.008	0.058	0.005	0.178	0.002	0.631	–2.00	0.63	0.09	0.28

Seasonally, we note that the overall backscatter of marshes and swamps is similar in June and September, but lower in November. This may be attributed to drying conditions in the fall. The proportions of the three backscatter mechanisms as attributed to odd bounce, even bounce, and volume scattering are similar for all three dates.

D. Discussion

Our polarimetric and interferometric observations of wetlands with the Radarsat-2 SAR sensor yield unexpected findings:

1) nearly identical fringe patterns in HH + VV, HH − VV, and HV over the Everglades [14];
2) co-pol phase differences that suggest single bounce rather than double bounce in the observed wetlands; and
3) polarimetric decomposition results that indicate odd-bounce returns that are substantially larger than the expected double (even)-bounce returns [15].

Several past papers have reported similar, puzzling findings. Airborne observations of dry corn on a smooth soil substrate by Ulaby *et al.* [24] showed a strong variability with incidence angle, with HH–VV phase angles of 20° at an incidence angle of 18° increasing rapidly to values near 120° for an incidence angle of 32°, and then declining slowly to values near 100° at an incidence angle of 52°. Non-180° co-pol phase differences were noted for Amazon floodplain forests with SIR-C data by Hess *et al*. [25]. More recently, experiments by Lopez-Sanchez *et al.* at X-band [26], [27] and C-band [28] have investigated the HH–VV phase differences from emerging rice at a variety of incidence angles. For incident angles of 30° or greater, the co-pol phase difference is 0° before emergence of the rice from the water, increases to 120°–130° after emergence, and slowly decreases back toward zero as the canopy develops. However, for a smaller (22°) incidence angle, the HH–VV phase remains near zero throughout the growing season.

Older [24] and recent theoretical results [29] may shed some light on HH–VV phase values near 0° in situations where double-bounce backscatter plays an important role. The sudden jump in phase observed in [24] was interpreted as a result of the change in the Fresnel reflection coefficient at the Brewster angle. With models supported by laboratory data, [29] showed that the HH–VV phase difference is strongly dependent on the incidence angle and moisture of columnar scatterers on a dielectric plane, thus providing a possible explanation for the anomalous observed phase discussed in this paper.

Our results, together with the above corroborating results, show the dangers of interpreting the outputs of decomposition models literally. It is apparent that HH–VV phase distributions provide important diagnostic information in wetland environments, but additional observations, interpreted with the help of reliable modeling, will be necessary to improve our understanding of the backscatter process. This work will be necessary to extract information of natural wetlands from polarimetric SAR data usefully and reliably.

IV. Conclusion and Recommendations

In this paper, we have inspected the HH–VV phase, calculated the Pauli coherency matrix, and implemented three polarimetric decompositions. All of these indicate that the odd-bounce mechanism dominates in both marsh and swamp wetlands. Yet, interferometric results in the Everglades [14] and in Ontario (to be published), as well as the HH/VV intensity ratio, indicate a double-bounce interaction with the water and the vegetation stems. The conclusion we draw is that wetland scattering includes a strong double-bounce component, which appears as single bounce when the HH–VV phase is used as a diagnostic criterion, due to an anomalous polarimetric response. As suggested by published observations and two modeling results [24] and [29], the incidence angle may be expected to play a critical role through its impact upon the co-pol phase difference. It is the intent of the authors to investigate the influence of incidence angle and other variables as they affect the polarimetric backscatter of selected test sites.

The key outcome of this research to date is to point out that current decomposition models may not be applicable to wetlands in some circumstances. All decompositions of the study areas indicated that the scattering was surface bounce, whereas we argue that the observations can only be explained in terms of double bounce from the vegetation and water surface. If wetlands are approached as being characterized by double-bounce backscatter, this will lead to a misclassification of the wetlands using traditional polarimetric decompositions. Clearly, parameters other than HH–VV phase need to be invoked to identify this double-bounce behavior. Additional observational and theoretical work is required to understand the backscatter physics, determine the intrinsic information provided by polarimetric data, and learn how to extract information of value for resource managers.

Acknowledgment

The authors are pleased to acknowledge the essential contribution of funding and data support from the Canadian Space Agency. They wish to acknowledge ongoing discussions with K. Raney and R. Touzi that have been consistently helpful. A review of earlier drafts by J. van der Sanden and subsequent discussions have contributed to this paper. The detailed and constructive comments by two JSTARS referees were also very beneficial.

References

[1] B. Brisco *et al.*, "Water resource applications with RADARSAT-2–a preview," *Int. J. Digital Earth*, vol. 1, no. 1, pp. 130–147, Jan. 2008.

[2] B. Brisco, N. Short, J. J. van der Sanden, R. Landry, and D. Raymond, "A semi-automated tool for surface water mapping with RADARSAT-1," *Can. J. Remote Sens.*, vol. 35, no. 4, pp. 336–344, Aug. 2009.

[3] B. Brisco, "Mapping and monitoring surface water and wetlands with SAR," in *Remote Sensing of Wetlands: Applications and Advances*, R. W. Tiner, M. Lang, and V. Klemas, Eds. Boca Raton, FL, USA: CRC Press/Taylor & Francis (Cat# K23165), 2015.

[4] J. Wang, J. Shang, B. Brisco, and R. Brown, "Evaluation of multidate ERS-1 and multispectral Landsat imagery for wetland detection in Southern Ontario," *Can. J. Remote Sens.*, vol. 24, no. 1 pp. 60–68, Jan. 1998.

[5] J. Toyra, A. Pietroniro, and L. Martz, "Multisensor hydrologic assessment of freshwater wetland," *Remote Sens. Environ.*, vol. 75, no. 2, pp. 162–173, Feb. 2001.

[6] M. Grenier *et al.*, "An object-based method to map wetlands using RADARSAT-1 and Landsat ETM images: Test case on two sites in Quebec, Canada," *Can. J. Remote Sens.*, vol. 33, no. S1, pp. S28–S45, Dec. 2007.

[7] J. Corcoran *et al.*, "The integration of optical, topographic, and radar data for wetland mapping in Northern Minnesota," *Can. J. Remote Sens.*, vol. 37, no. S1, pp. 564–582, Dec. 2011.

[8] M. Koch, T. Schmid, M. Reyes, and J. Gumuzzio, "Evaluating full polarimetric C- and L-band data for mapping wetland conditions in a semi-arid environment in Central Spain," *IEEE J. Sel. Topics Appl. Earth Observ. Remote Sens.*, vol. 5, no. 3, pp. 1033–1044, Jun. 2012.

[9] L. L. Hess, J. M. Melack, and D. S. Simonett, "Radar detection of flooding beneath the forest canopy: a review," *Int. J. Remote Sens.*, vol. 11, no. 7, pp. 1313–1325, Jul. 1990.

[10] K. O. Pope, E. Rejmankova, J. F. Paris, and R. Woodruff, "Detecting seasonal flooding cycles in marshes of the Yucatan Peninsula with SIR-C polarimetric radar imagery," *Remote Sens. Environ.*, vol. 59, no. 2, pp. 157–166, Feb. 1997.

[11] E. S. Kasischke and L.L. Bourgeau-Chavez, "Monitoring South Florida wetlands using ERS-1 SAR imagery," *Photogramm. Eng. Remote Sens.*, vol. 63, no. 3, pp. 281–291, Mar. 1997.

[12] P. A. Townsend, "Relationship between forest structure and the detection of flood inundation in forested wetlands using C-band SAR," *Int. J. Remote Sens.*, vol. 23, no. 3, pp. 443–460, Feb. 2002.

[13] F. M. Henderson and A. J. Lewis, "Radar detection of wetland ecosystems: a review," *Int. J. Remote Sens.*, vol. 29, no. 20, pp. 5809–5835, Oct. 2008.

[14] S.-H. Hong and S. Wdowinski, "Double bounce component in cross-polarimetric SAR from a new scattering target decomposition," *IEEE Trans. Geosci. Remote Sens.*, vol. 52, no. 6, pp. 3039–3051, Jun. 2014.

[15] F. Ahern, "Polarimetric Backscatter characteristics of wetland and non-wetland land cover types in the Lake Clear Study area," TerreVista Earth Imaging, Cormac, Ontario, Contract Rep. to Canada Centre for Remote Sensing, Feb. 2014.

[16] J. J. Van Zyl, "Unsupervised classification of scattering behavior using radar polarimetry data," *IEEE Trans. Geosci. Remote Sens.*, vol. 27, no. 1, pp. 36–45, Jan. 1989.

[17] D. Atwood *et al.*, "Wave propagation model for coherent scattering from a randomly distributed target," in *Proc. 6th Int. Workshop Sci. Appl. SAR Polarimetry Polarimetric Interferometry (POLinSAR'13)*, Frascati, Italy, Jan. 28–Feb. 1, 2013, 6 p.

[18] W. Boerner, "Basic concepts in radar polarimetry," *PolSARpro V3.0*, Frascati, Italy: European Space Agency, [Online]. Available: http://earth.eo.esa.int/polsarpro/Manuals/LN_Basic_Concepts.pdf

[19] European Space Agency. (2013). *PolSarPro, Tutorial on Radar Polarimetry: Polarimetric Decompositions, in Polarimetry Tutorial* [Online]. Available: http://earth.eo.esa.int/polsarpro/Manuals/4_Polarimetric_Decompositions.pdf, Downloaded Aug. 10, 2013.

[20] A. Freeman and S. L. Durden, "A three-component scattering model for polarimetric SAR data," *IEEE Trans. Geosci. Remote Sens.*, vol. 36, no. 3, pp. 963–973, May 1998.

[21] R. K. Raney, J. T. S. Cahill, G. W. Patterson, and D. B. J. Bussey, "The m-chi decomposition of hybrid dual-polarimetric radar data with application to lunar craters," *J. Geophys. Res.*, vol. 117, no. E00H21, p. 8, May 2012.

[22] R. K. Raney, "A perspective on compact polarimetry," *IEEE Geosci. Remote Sens. Newsletter*, vol. 160, pp. 12–18, Sep. 2011.

[23] Y. Yamaguchi, T. Moriyama, M. Ishido, and H. Yamada, "Four-component scattering model for polarimetric SAR image decomposition," *IEEE Trans. Geosci. Remote Sens.*, vol. 43, no. 8, pp. 1699–1706, Aug. 2005.

[24] F. T. Ulaby, D. Held, M. C. Dobson, K. C. McDonald, and T. B. A. Senior, "Relating polarization phase difference of SAR signals to scene properties," *IEEE Trans. Geosci. Remote Sens.*, vol. 25, no. 1, pp. 83–92, Jan. 1987.

[25] L. L. Hess, J. M. Melack, S. Filoso, and Y. Wang, "Delineation of inundated area and vegetation along the Amazon floodplain with the SIR-C synthetic aperture radar," *IEEE Trans. Geosci. Remote Sens.*, vol. 33, no. 4, pp. 896–904, Jul. 1995.

[26] J. M. Lopez-Sanchez, S. R. Cloude, and J. D. Ballester-Berman, "Rice phenology monitoring by means of SAR polarimetry at X-band," *IEEE Trans. Geosci. Remote Sens.*, vol. 50, no. 7, pp. 2695–2709, Jul. 2012.

[27] J. M. Lopez-Sanchez, F. Vicente-Guijalba, J. D. Ballester-Berman, and S. R. Cloude, "Influence of incidence angle on the coherent copolar polarimetric response of rice at X-band," *IEEE Geosci. Remote Sens. Lett.*, vol. 12, no. 2, pp. 249–253, Feb. 2015.
[28] J. M. Lopez-Sanchez, F. Vicente-Guijalba, J. D. Ballester-Berman, and S. R. Cloude, "Polarimetric response of rice fields at C-band: analysis and phenology retrieval," *IEEE Trans. Geosci. Remote Sens.*, vol. 52, no. 5, pp. 2977–2993, May 2014.
[29] T. Watanabe *et al.*, "Experimental study of effects of forest moisture on polarimetric radar backscatter," in *Proc. Int. Geosci. Remote Sens. Symp. 35th Can. Symp. Remote Sens.*, Québec, Canada, Jul. 2014, 4 p.

Brian Brisco received the B.Sc. degree in ecology and the M.Sc. degree in soil science from the University of Guelph, Guelph, ON, Canada, in 1977 and 1980, respectively, and the Ph.D. degree in remote sensing/physical geography from the University of Kansas, Lawrence, KS, USA, in 1985.

He has been involved in remote sensing since 1975 and participated in the SURSAT project from 1977 to 1980. He worked as a National Science and Engineering Research Council Fellow with the Canada Centre for Remote Sensing (CCRS), Ottawa, ON, Canada, from 1986 to 1989, with Intera Remote Sensing from 1989 to 1997, and with Noetix Research Inc., Ottawa, ON, Canada, from 1997 to 2004, where he was the Director of Research and Applications Development. In 2004, he joined CCRS as a Research Scientist. He has authored or co-authored more than 200 publications including over 50 peer reviewed journal publications and is the author of two chapters in the Manual of Remote Sensing volume on radar applications published by American Society of Photogrammetry and Remote Sensing. His extensive publications include studies on vegetation characterization, crop identification and monitoring, conservation farming/ soil erosion mapping, soil moisture estimation, land cover mapping, wetland mapping, rangeland management, forestry, and developing tools and techniques for ground truth data acquisition. His research interests include interferometry, polarimetry, and radar backscatter modeling including software development and operational implementation, and remote sensing, particularly synthetic aperture radar (SAR), for mapping and managing renewable resources.

Dr. Brisco is a member and Past President of the Canadian Remote Sensing Society.

Frank Ahern received the A.B. degree in physics and mathematics from Cornell University, Ithaca, NY, USA, in 1966, and the Ph.D. degree in astrophysics from the University of Maryland, College Park, MD, USA, in 1972.

After two years, he was with the University of Toronto, Toronto, ON, Canada, as a National Science and Engineering Research Council Fellow from 1972 to 1974. He joined the Canada Centre for Remote Sensing (CCRS), Ottawa, ON, Canada, as a Research Scientist in 1975, where he remained until 2000. He has authored or co-authored 55 articles in refereed journals, 5 books (as author, editor, or chapter author), and over 120 additional publications. His research interests include radiometric corrections of Landsat data, optical spectrometry, atmospheric corrections, and development of applications of remote sensing data for rangeland and forestry.

Dr. Ahern is a member of the Canadian Remote Sensing Society and served as the Editor in Chief of the *Canadian Journal of Remote Sensing* from 1985 to 1990. He was awarded the Gold Medal of the Canadian Remote Sensing Society for 1991.

Sang-Hoon Hong (S'03–M'07) received the B.S. and M.S. degrees in geological sciences and the Ph.D. degree in earth system sciences from Yonsei University, Seoul, Korea, in 1997, 1999, and 2006, respectively.

He is currently working as a Senior Research Scientist with Korea Polar Research Institute, Incheon, Korea. He was a Senior Researcher with the Satellite Information Research Center, Korea Aerospace Research Institute, Daejeon, Korea. He was a Postdoctoral Researcher with the Division of Marine Geology and Geophysics, University of Miami, Miami, FL, USA, and also with the College of Engineering and Computing, Florida International University, Miami, FL, USA. His research interests include radar interferometry, radar polarimetry, and microwave signal processing. He applied these SAR, InSAR, and PolSAR techniques for the study of geophysical parameter retrieval and geodetic change observation.

Dr. Hong is a Principal Investigator of projects supported by the German Aerospace Center (DLR) and Japan Aerospace Exploration Agency (JAXA) for research using SAR observations.

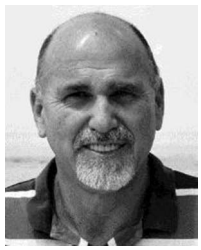

Shimon Wdowinski received the B.Sc. degree in earth sciences and the M.Sc. degree in geology from the Hebrew University, Jerusalem, Israel, in 1983 and 1985, respectively; the M.S. degree in engineering sciences and the Ph.D. degree in geophysics from Harvard University, Boston, MA, USA, in 1987 and 1990, respectively.

Before resuming a faculty position at Tel Aviv University, Tel Aviv, Israel, in 1994, he conducted a post-doctorate research at Scripps Institute of Oceanography, University of California at San Diego, La Jolla, CA, USA, from 1990 to 1993. He joined the Department of Marine Geosciences, University of Miami, Miami, FL, USA, in 2004.

Kevin Murnaghan received the B.Sc. degree (Hons.) in applied physics with a minor in computer science from Waterloo University, Waterloo, ON, Canada, in 1996.

Since 1997, He has been worked with the Canada Centre for Remote Sensing, Ottawa, ON, Canada.

Lori White received the B.Sc. degree (Hons.) in biology from Dalhousie University, Halifax, Nova Scotia, in 2001, Diploma degree in GIS from the Centre for Geographic Sciences, Lawrencetown, Nova Scotia, in 2003, and the M.Sc. degree in biology from the University of Ottawa, Ottawa, ON, Canada, in 2013.

She joined the Canada Centre for Remote Sensing (CCRS), Ottawa, ON, Canada, as an Environmental Scientist in 2008. Her research interests include RADARSAT-2 data to investigate their use in mapping and monitoring surface water, flooded vegetation, wetland characterization, and invasive plants.

Donald K. Atwood (M'95) received the Ph.D. degree in physics from the Massachusetts Institute of Technology (MIT), Cambridge, MA, USA.

He was with the AT&T Bell Laboratories, Murray Hill, NJ, USA and Raytheon's Research Division, Lexington, MA, USA, where he worked in the field of microlithography. In 1992, he joined MIT Sea Grant, Cambridge, MA, USA, where he developed autonomous underwater vehicles with specialization in underwater acoustics. Then he worked for Raytheon, Waltham, MA, USA, first as a Technical Advisor for International Environmental Programs, then as a Manager in atmospheric remote sensing at the Goddard Space Flight Center, Greenbelt, MD, USA. In 2000, he became the Director of Science Support for the U.S. Antarctic Program. Next, he served as a Chief Scientist with the Alaska Satellite Facility (ASF), University of Alaska Fairbanks, Fairbanks, AK, USA, where he focused on applications of SAR, PolSAR, and interferometry for Earth Science. Currently, he is a Senior Research Scientist with Michigan Tech Research Institute, Ann Arbor, MI, USA, where he works on defense and environmental programs.

Dr. Atwood is a member of the American Geophysical Union and the American Society of Photogrammetry and Remote Sensing.